Intraseasonal Interactions between Temperature and Vegetation over the Boreal Forests

Weile Wang* and Bruce T. Anderson

Department of Geography and Environment, Boston University, Boston, Massachusetts

Dara Entekhabi

Ralph M. Parsons Laboratory, Department of Civil and Environmental Engineering, Massachusetts Institute of Technology, Cambridge, Massachusetts

Dong Huang, Yin Su, Robert K. Kaufmann, and Ranga B. Myneni

Department of Geography and Environment, Boston University, Boston, Massachusetts

Received 22 September 2006; accepted 19 April 2007

ABSTRACT: This paper uses statistical and analytical techniques to investigate intraseasonal interactions between temperature and vegetation [surrogated by the normalized difference vegetation index (NDVI)] over the boreal forests. Results indicate that interactions between the two fields may be approximated as a coupled second-order system, in which the variability of NDVI and temperature of the current month is significantly regulated by lagged NDVI anomalies from the preceding two months. In particular, the influence from the one-month lagged NDVI anomalies upon both temperature and vegetation

* Corresponding author address: Weile Wang, Foundation of California State University—Monterey Bay/NASA Ames Research Center, Moffett Field, CA 94035.
E-mail address: weile.wang@gmail.edu

DOI: 10.1175/EI219.1

variability is generally positive, but the influence from the second-month lagged NDVI anomalies is often negative. Such regulations lead to an intrinsic oscillatory variability of vegetation at growing-season time scales across the study domain. The regulation of temperature variability by NDVI anomalies is most significant over interior Asia (Siberia), suggesting strong vegetation–atmosphere couplings over these regions. Physical mechanisms for these statistical results are investigated further with a stochastic model. The model suggests that the oscillatory variability of the temperature–NDVI system may reflect the dynamic adjustments between the two fields as they maintain a thermal balance within the soil and lower boundary layer of the atmosphere; the particular role vegetation plays in this scenario is mainly to dissipate heat and therefore reduce surface temperatures.

KEYWORDS: Land–atmosphere interaction; Remote sensing; Modeling

1. Introduction

Terrestrial vegetation covers more than 70% of the Earth's land surface and can be looked at as one of many dynamic interfaces between the land and the atmosphere. On the one hand, vegetation is strongly controlled by climate, and thus variations in surface temperature, precipitation, and solar radiation will cause subsequent variations in vegetation (e.g., Budyko 1974; Walter 1985; Woodward 1987). On the other hand, because vegetation plays an active role in regulating exchanges of energy, mass, and momentum between the surface and the atmosphere, disturbances of vegetation in turn affect climate variability at various temporal–spatial scales (e.g., Sellers et al. 1997; Pielke et al. 1998). These coupled interactions characterize the basic relationship between vegetation and the climate.

The use of satellites to monitor global vegetation activity in the past two decades has greatly facilitated the study of vegetation–climate interactions. Extensive research has investigated the impacts of recent climate variations on the Earth's biosphere. For instance, analyses of normalized difference vegetation index (NDVI) datasets indicate that forested vegetation between 40° and 70°N has increased significantly since the early 1980s (Braswell et al. 1997; Myneni et al. 1997; Zhou et al. 2001). These greening forests show a strong correlation with the pronounced warming of surface temperatures in these regions (Hansen et al. 1999) and coincide with major modes of global climate variability [namely, the El Niño–Southern Oscillation (ENSO) and the Arctic Oscillation (AO)] in their spatial–temporal patterns (Buermann et al. 2003). These observed vegetation variations are also reproduced by numerical vegetation models (e.g., Lucht et al. 2002), which further suggest that satellite datasets can capture large-scale vegetation dynamics.

Because the observed variations of vegetation and climate are the results of their coupled interactions, the above studies suggest that satellite datasets may also provide information for studying large-scale vegetation feedbacks on climate variability. Recently, some studies tried to address this question using correlation-based statistical techniques (e.g., Brunsell 2006; Liu et al. 2006; Notaro et al. 2006). For instance, Liu et al. (Liu et. al 2006) and Notaro et al. (Notaro et al. 2006) used lead/lag correlations and a statistical metric previously applied to ocean–atmosphere feedbacks (Frankignoul et al. 1998) to assess vegetation–climate feedbacks in satellite-sensed fraction of photosynthetically actively ra-

diation (FPAR) datasets and observational climate records. They identified significant positive correlations between anomalies of surface temperature and FPAR from the preceding month over the boreal regions, which, as suggested by the authors, may reflect vegetation's positive feedbacks on climate variability via the albedo pathway (Liu et al. 2006; Notaro et al. 2006).

However, the internal variability of climate is known to be very complicated, while the influence of vegetation on the overlying atmosphere may not be as strong as the ocean–atmosphere couplings. In addition, systematic observations for land surface processes are very limited (for instance, this study, and the above referenced studies, only use datasets for vegetation, surface temperature, and precipitation). Due to these limitations, climate variations often appear to be highly "random" in statistical analyses: only a small portion of their variance can generally be explained, and explanatory power provided by vegetation is even more limited (see below). As such, it is generally difficult to distinguish the weak influence of vegetation on climate variability based on simple correlations alone. In addition, there remains the challenge of interpreting the statistical results, if any, so that they are physically meaningful.

In an attempt to address these problems, Wang et al. (Wang et al. 2006a, hereafter W1; Wang et al. 2006b, hereafter W2) developed a set of methodologies to investigate interactions between monthly anomalies of NDVI, surface temperature, and precipitation over the North American Grasslands. These methodologies are based around a statistical definition of causality, namely, Granger causality (Granger 1969; Granger 1980). According to this definition, vegetation is said to "Granger cause" climate variability if and only if lagged (i.e., past) NDVI anomalies provide *unique* information about future climate variations (W1). Here, the word "unique" is emphasized because it requires that the information provided by vegetation cannot be obtained from other variables (e.g., lagged anomalies of temperature and precipitation) in the information set (Granger 1969; Kaufmann and Stern 1997; Wang et al. 2004). That is, if we can identify a component of climate variability that is uniquely associated with characteristics of vegetation variability, weak as it may be, it will provide reliable evidence for vegetation feedbacks.

To determine the characteristic variability of vegetation in turn requires understanding how vegetation dynamically responds to climate forcing. For the North American Grasslands, precipitation is known to be the major climatic constraint of vegetation growth; however, the analyses of W1 indicate that vegetation's response to precipitation variations is time scale dependent. In particular, vegetation–precipitation coupling has an intrinsic oscillatory component at intraseasonal time scales (around the eight-month period). Because of this oscillatory variability, higher (lower) NDVI anomalies earlier in the season tend to be followed by lower (higher) NDVI anomalies several months later (W1). This characteristic variability is also detected in the causal relationships from vegetation to climate variations, which indicate that higher (lower) initial NDVI anomalies may Granger cause lower (higher) precipitation anomalies later in the summer (W1).

The findings of W1 allowed us to develop a stochastic model to describe interactions among vegetation, soil moisture, and precipitation over the midlatitude grasslands (W2). By relating vegetation variability to the balance of soil moisture and precipitation, the model captures the observed characteristics of the

vegetation–climate interactions discussed above. In particular, analyses of the model indicate that interactions between vegetation and soil moisture can generate oscillatory adjustments between the two fields: the faster vegetation grows (in response to water surplus), and the longer the vegetation anomalies persist, the more likely the system will be to generate intraseasonal oscillations (W2). These land surface signals can then feed back to the atmosphere via the known soil moisture–precipitation couplings in this region (Koster et al. 2004; W2). As such, the model of W2 provides a clearer physical interpretation for its statistical counterpart estimated in W1.

Although these preceding analyses principally focus on midlatitude grasslands, the methodologies developed in them may have broader applications in other regions. For boreal forests, for instance, many studies have shown that vegetation there is largely regulated by variations in surface temperature (e.g., Myneni et al. 1997; Zhou et al. 2001; Zhou et al. 2003). However, the intrinsic variability of these forests at intraseasonal time scales is less well studied. Also, the link between vegetation variability and vegetation feedbacks has not been emphasized in the literature. Do these forests display some distinct intraseasonal vegetation variability? And will such characteristic vegetation signals be detectable in temperatures? These are the questions this study aims to investigate.

This paper is structured as follows. Section 2 introduces the datasets used in the analyses and how they are compiled. Section 3 applies the methodologies of W1 to analyze the observed covariability between vegetation and temperature over the boreal forests. In particular, it shows that similar to grasslands, vegetation–climate interactions over the forests can be captured by a pair of second-order statistical equations. Based on these statistical results, section 4 extends the model of W2 to explain the eco-physical mechanisms for the observed variability and discusses its biogeophysical implications. Finally, our conclusions are presented in section 5.

2. Datasets and compilation

This study uses the temperature dataset from the National Aeronautics and Space Administration (NASA) Goddard Institute for Space Studies (GISS) surface temperature analysis (Hansen et al. 1999; Hansen et al. 2001), the precipitation dataset from the National Oceanic and Atmospheric Administration (NOAA) Climate Prediction Center (CPC) Merged Analysis of Precipitation (CMAP; Xie and Arkin 1997), and the NDVI dataset derived from the NOAA Advanced Very High Resolution Radiometer (AVHRR) instruments by the Global Inventory Monitoring and Modeling Studies group (GIMMS; Tucker et al. 2005). These datasets have satisfied several quality criteria and have been used in many previous analyses (e.g., Buermann et al. 2003; Kaufmann et al. 2003; Lotsch et al. 2003; Zhou et al. 2001; Zhou et al. 2003). More detailed descriptions of these datasets can also be found in W1.

For all datasets, only data for the boreal growing season (April–October) during the period of 1982–2000 are used. The domain of the analysis (Figure 1) is defined as land surfaces between 40° and 75°N, where 1) all the surface temperature, precipitation, and NDVI data are available; 2) the grid point has a valid vegetation type (e.g., "forest") as determined by a land cover map derived from Friedl et al. (Friedl et al. 2002); and 3) values of NDVI are always equal to or greater than 0.1

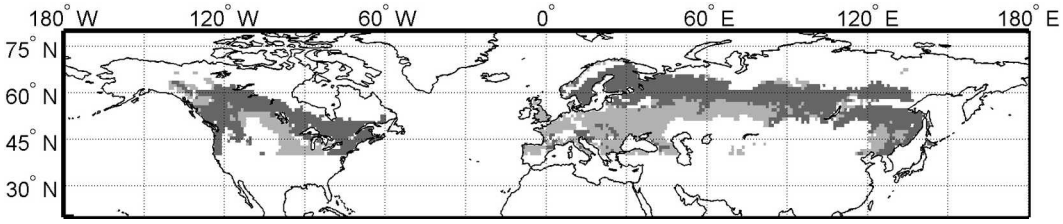

Figure 1. The domain for this analysis (shaded areas). The dark shades indicate boreal forests over North America and Eurasia, where grid points are compiled together into two panels, respectively. The light shades indicate regions that are not classified as forests but are also included in the spatial analysis. Regions classified as grasslands are excluded from the analysis. Vegetation types are determined by a land cover map derived from Friedl et al. (2002).

in every growing-season month during the analyzed period. Low NDVI values are excluded because they may represent pixels covered by surface snow and ice, which would introduce errors. In addition, because this paper focuses on forests, we also exclude grasslands from the analysis. For each grid point, monthly anomalies of NDVI, temperature, and precipitation are calculated relative to their 1982–2000 averages (i.e., the mean seasonal cycle).

This study will consist of two different types of analyses, and thus we compile time series in two corresponding ways. The first analyzes climate–vegetation interactions for each of the growing-season months. A panel-data approach (W1) is used to help increase the size of the data samples and the degrees of freedom of this analysis. That is, we group grid points that have the biome type of forests (Friedl et al. 2002) into two panels for North America (NA) and Eurasia (EA). In this approach, NDVI data are first aggregated to 2° × 2° grid points to match the resolution of the climate records. To avoid possible correlations among the data, we then choose one 2° × 2° grid point from every 4° × 4° block cell such that the resampled data are not spatially adjacent to each other. The final panels organized for NA and EA have about 40 and 70 grid points, respectively. For every month of the growing season, therefore, we have 40 × 19 (NA) or 70 × 19 (EA) degrees of freedom.

In the second analysis, we try to determine the spatial pattern of these climate–vegetation interactions. In this case, the full gridpoint time series are compiled by linking the seven (April–October) monthly anomalies during a growing season to the seven monthly anomalies during the next growing season. This approach extends the data length of each time series to 133 months (7 growing-season months × 19 yr from 1982 to 2000). Compiling the data this way assumes that the vegetation–climate interactions do not vary during the growing season, such that NDVI (temperature/precipitation) anomalies from the preceding month have the same influence on current temperature/precipitation (NDVI) variations, regardless of the calendar month (March, April, etc.). In addition, because it concatenates seven observations from one year with observations from the previous and subsequent year, the gridpoint time series itself is not continuous. This discontinuity

implies that lagged values should not include months from the previous year. As a result, statistical models that specify a one-month lag eliminate 19 observations (one month for each year) from the sample. In this spatial-analysis approach the temperature and the precipitation datasets are reprojected to 1° × 1° grid cells to match the spatial resolution of the NDVI dataset.

Finally, we want to emphasize that the analyses and the results of this study are based on monthly anomalies of these variables, although in places where this reference is clear, the use of the term "anomalies" or "variations" may be omitted in order to avoid lengthy repeats.

3. Observed vegetation/temperature covariability

The analyses of W1 and W2 indicate that vegetation–climate interactions over the semiarid grasslands can be described by a pair of second-order difference equations as follows:

$$V'_t = A_1 V'_{t-1} + A_2 V'_{t-2} + A_3 P'_{t-1} + \varepsilon_{1t}, \tag{1}$$

$$P'_t = B_1 V'_{t-1} + B_2 V'_{t-2} + B_3 P'_{t-1} + \varepsilon_{2t}, \tag{2}$$

where V' and P' represent anomalies of vegetation and precipitation, respectively; As and Bs are constant regression coefficients; and εs are errors. The subscript t stands for the month of interest and $t - 1$, for instance, denotes the preceding month. Note that Equations (1) and (2) do not include a constant on the right-hand side of the equations. This is because all the variables here are anomalies with a zero mean, and thus this constant regressor, if included, will be zero by definition (Stock and Watson 2003). For the same reason, other statistical models discussed throughout this paper will not contain a constant regressor.

Equations (1) and (2) are referred to as the climate-forcing equation and the feedback equation, respectively. As written, Equation (1) indicates that the current variability of vegetation depends not only on the climate forcing (i.e., precipitation) but also on its own values from the preceding *two* months. Because these lagged vegetation terms determine the intrinsic variability of vegetation, they are also included in Equation (2) to help detect the impact of vegetation on climate variability. A physical explanation for the use of a one-month lagged precipitation term (P'_{t-1}) in Equation (1) is based on our previous finding that over the North American Grasslands, variations of NDVI most strongly respond to precipitation anomalies from the preceding month (W1). This is also consistent with findings of other studies in the literature (e.g., Liu et al. 2006). Detailed derivations and discussions of Equations (1) and (2) can be found in W2.

Analogous to the above equations, this section extends the form of Equations (1) and (2) to investigate the vegetation–climate interactions over the boreal forests. Explanations for this generalization will be discussed in the next section.

3.1. Vegetation variability driven by climate

Because the growth of boreal forests is regulated by temperatures, we replace the precipitation term in Equation (1) with temperatures as follows:

$$V'_t = A_1 V'_{t-1} + A_2 V'_{t-2} + A_3 T'_t + \varepsilon_{1t}, \tag{3}$$

where T'_t represents temperature anomalies. Note that Equation (3) uses T'_t, instead of T'_{t-1}, to determine current vegetation variability. This is because many biochemical processes are very sensitive to temperature variations, and their responses are almost instantaneous at monthly time scales. Indeed, preliminary analyses find that the strongest correlations are between concurrent temperature and NDVI anomalies over these regions (not shown).

To examine whether Equation (3) captures vegetation dynamics over the boreal forests, we regress it against the two panel data compiled for North America and Eurasia (Table 1). For both continents, the r^2 statistics of the regressions are above 40% for almost all the months during June through October (Table 1). For a model as simple as Equation (3), this represents a fairly high explanatory power of the NDVI anomalies (see below). In addition to the r^2 values, the estimated regression coefficients also show a regular pattern in which values of A_1 and A_3 are always positive, and those for A_2 are always negative (all of them are significant at the 99% level; Table 1). Because A_1 and A_3, respectively, represent the persistence of vegetation anomalies and the influence of temperatures on vegetation, the positive values are expected. At the same time, the negative values for A_2 indicate that vegetation anomalies from two months earlier have a negative impact on its current status, which suggests the possibility of intraseasonal oscillations (W2; also see below).

To assess whether the results of Table 1 are influenced by possible seasonality contained in the size of monthly anomalies of vegetation and temperature, we repeat the regression by normalizing these anomalies so that they have the same standard deviations (for vegetation and temperature, respectively) during the growing season. Results indicate that the regression coefficients estimated using these normalized anomalies (not shown) are consistent with those of Table 1, which suggests that the seasonality in the original anomalies is generally weak and thus does not have a significant impact on the regression analyses. Therefore, we will discuss the results obtained using the full monthly anomalies.

It is of interest to compare the results of Table 1 with those from previous

Table 1. Regression coefficients of the climate forcing equation (Equation (3)) estimated based on monthly anomalies of temperature and NDVI over boreal forests in (a) North America and (b) Eurasia. Also shown are the r^2 statistics of the regressions. All values are statistically significant at the 99% level ($p < 0.01$).

	A_1	A_2	A_3(×100)	r^2
		(a) North America		
Jun	0.77	–0.41	0.48	0.51
Jul	0.65	–0.36	0.57	0.47
Aug	0.85	–0.28	0.17	0.53
Sep	0.88	–0.23	0.45	0.50
Oct	0.85	–0.35	0.48	0.41
		(b) Eurasia		
	A_1	A_2	A_3(×100)	r^2
Jun	0.68	–0.34	0.78	0.62
Jul	0.59	–0.26	0.19	0.34
Aug	0.88	–0.30	0.34	0.49
Sep	0.84	–0.18	0.16	0.44
Oct	0.76	–0.36	0.35	0.49

studies. In particular, Zhou et al. (Zhou et al. 2003) used a rather complicated (e.g., nonlinear) statistical model to estimate the effects of climate factors on vegetation variability, and captured about 10%–33% of the variance of NDVI anomalies over the boreal forests. In comparison, this study captures a higher proportion (>40%) of the variance with a simpler (linear) model [Equation (3)]. The main advantage of this model is the inclusion of lagged NDVI anomalies to explain their future variability. This approach is consistent with the fact that vegetation growth depends on its previous status; in addition, because lagged NDVI anomalies represent accumulated effects of past climate conditions on vegetation growth, including them into the model also removes the need to specify such lagged climate influence explicitly. On the other hand, in order to make the analysis simple, this study has neglected some uncertainties associated with the data (e.g., spatial variability between the grid cells). These uncertainties, as well as statistical techniques to address them, are discussed in Zhou et al. (Zhou et al. 2003). By utilizing the techniques described in Zhou et al. (Zhou et al. 2003), it may be possible to improve the regression results presented in Table 1. However, because the subject of this study is not to produce the optimal model but to use the model to identify important biophysical interactions within the vegetation–climate system, we will not incorporate them here.

To validate the regression results of Table 1, we use Equation (3) to reproduce the observed vegetation variations. That is, based on observations of current temperature anomalies (T'_t) and two lagged NDVI anomalies (V'_{t-1} and V'_{t-2}), Equation (3) is used to calculate the "expected" vegetation anomalies for the current month (V'_t). To simplify the calculation, we reestimated the three coefficients of Equation (3) based on the assumption that vegetation–climate interactions do not vary during the growing season, so that they can be characterized by the same set of parameters. The estimated parameters are 0.74, −0.32, and 0.005, respectively. (These values are representative of the results in Table 1 and will also be used in the examples throughout the paper.) Figure 2 shows the observed and the reproduced NDVI anomalies averaged over the two study sites. As shown, the model calculations match the observations with r^2 values of 0.60 and 0.68 for North America and Eurasia, respectively (Figure 2). These results are consistent with the regression analysis described above, although the r^2 values are larger because the spatial averaging of gridpoint time series reduces some of the noise associated with intergrid cell variability.

Another way to examine the temperature–vegetation covariability is to calculate the frequency response functions of the temperature–vegetation system. Simply speaking, the frequency response functions describe the magnitudes and phase angles of the outputs (NDVI) relative to the sinusoidal inputs (temperature) at different frequencies (Jenkins and Watts 1968). The frequency response functions can be analytically estimated based on Equation (3) and its estimated coefficients (W2). In addition, they can also be estimated directly from the observations without prior knowledge of Equation (3). This can be done by calculating the Fourier spectra of temperature and NDVI anomalies over every growing season, and then estimating the correlation coefficients between these spectra at different frequencies (or periods; W1). Because these correlation coefficients have complex values in general, they contain both magnitude (i.e., the gain function) and phase relationships between the two fields.

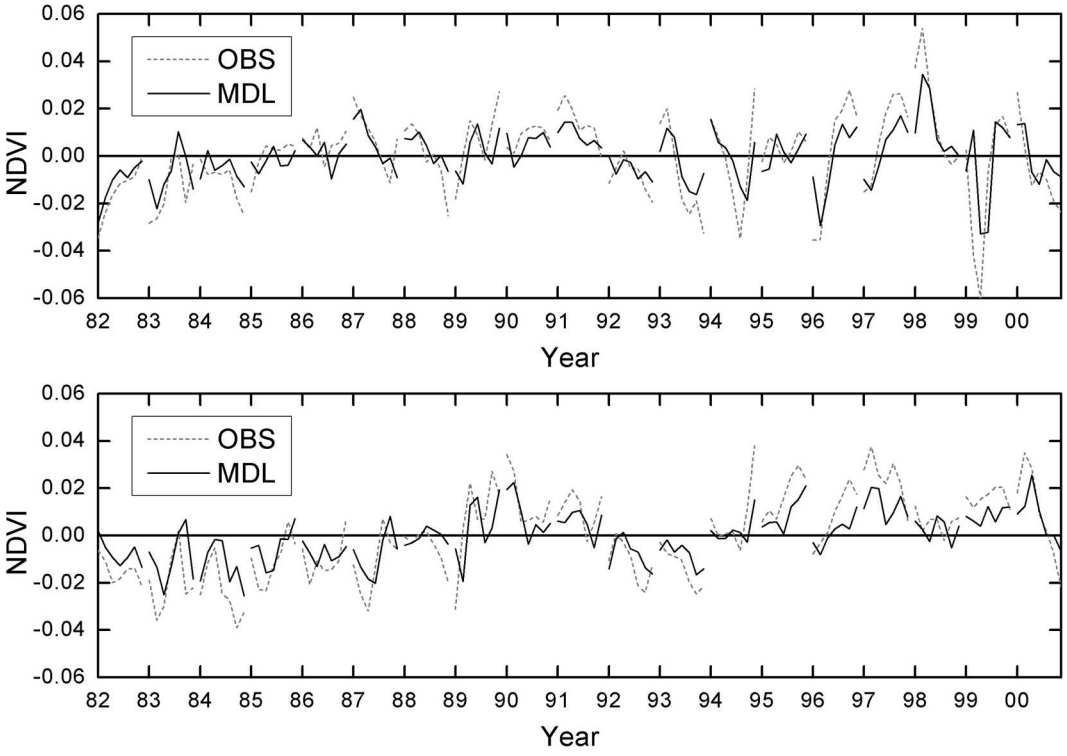

Figure 2. Area-averaged NDVI time series (anomalies) for boreal forests over (top) North America and (bottom) Eurasia. The dotted lines show observations and the solid lines show values from model calculations. In the calculations the coefficients of Equation (3) are set to 0.74, –0.32, and 0.005, respectively.

Figure 3 shows the frequency response functions estimated analytically from Equation (3) (the solid line) and those directly estimated from observations (the discrete dots for North America, and the crosses for Eurasia). For the convenience of comparison, the gain functions (Figure 3, top) are normalized by the input gain factor (A_3). Overall, Figure 3 indicates that the response functions estimated by both methods are consistent with one another. As shown, the gain functions indicate that vegetation has "red" responses to the temperature forcing: their magnitudes are positive (~4 dB) at time scales longer than 8 months, but decrease to negative values as the time scales become shorter (about −5 dB at the 2-month period); there is also a slight peak of the magnitudes at about the 7-month period (Figure 3, top). Such red magnitude characteristics are similar to the responses of vegetation to precipitation over the grasslands (W1; W2). On the other hand, the phase angles between temperature and NDVI anomalies are generally small, with a maximum phase lag of about −45° at the 4-month period (Figure 3, bottom). The phase characteristics reflect the fact that precipitation variations have a more persistent impact (via soil moisture storage) upon vegetation activity than do temperature variations (W1; W2).

The regression analysis and the frequency analysis above indicate that Equation

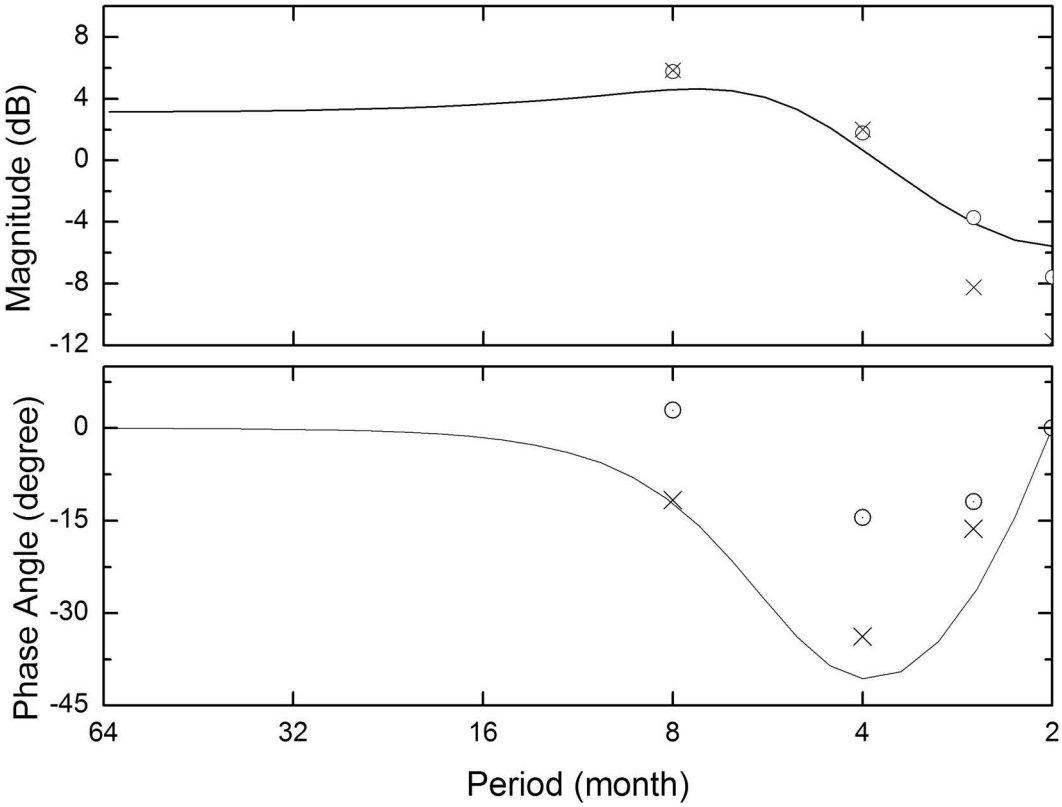

Figure 3. Estimated frequency response functions for the temperature–vegetation system over boreal forests. The discrete dots (for North America) and the crosses (for Eurasia) indicate estimates directly calculated from observations. The solid lines indicate the estimates analytically calculated from Equation (3), with the coefficients set to 0.74, –0.32, and 0.005, respectively. The gain functions are normalized by a factor of 0.005.

(3) captures the observed variability of vegetation as driven by temperature anomalies. In addition, they suggest that boreal forests also have intrinsic oscillatory variability at intraseasonal time scales. Such oscillatory variability can be quantitatively examined by the characteristic roots of Equation (3), which are given by the following formula:

$$\lambda_{1,2} = \frac{A_1 \pm \sqrt{\Delta}}{2}, \tag{4}$$

where

$$\Delta = A_1^{\,2} + 4A_2. \tag{5}$$

When the characteristic roots have complex components ($\Delta < 0$), this system will have intrinsic oscillatory variability.

Because the estimated coefficient A_2 is always negative (Table 1), a quick check of Equation (5) suggests that values of Δ can be negative and thus the system can

be oscillatory. By substituting A_1 and A_2 in Equation (4) with the estimated parameters (0.74 and –0.32; see the example of Figure 2), the formula gives two complex characteristic roots at exp(–0.57 ± *i*0.86). The imaginary part of the exponential indicates an oscillation frequency at 0.86 (rad month^{-1}), or equivalently at a period of 7.32 months. The real part of the exponential indicates that the magnitude of the oscillations decays at a rate of $e^{-0.57}$ per month; equivalently the time constant (or *e*-folding time) of such decaying processes is about 1.75 months.

The above results indicate oscillatory variability of vegetation over the boreal forests. As mentioned, similar results have also been reported over the midlatitude grasslands (in North America, in particular; W1; W2). Together, these results suggest that oscillatory variability may be a general feature of large-scale vegetation dynamics across broad regions and biomes. A physical mechanism for such variability will be discussed in detail in section 4.

3.2. Vegetation feedbacks

Similar to the analyses of the climate forcing equation, we also try to detect the influence of vegetation on temperature variability using the feedback equation:

$$T'_t = B_1 V'_{t-1} + B_2 V'_{t-2} + B_3 T'_{t-1} + \varepsilon_{2t}, \tag{6}$$

where *B*s are constant regression coefficients.

It is clear that Equation (6) has a similar form to the climate forcing equation, Equation (3). A qualitative explanation for this similarity is as follows. At monthly time scales, direct feedbacks of vegetation (e.g., albedo, evapotranspiration, etc.) mainly influence the variations of temperature at the concurrent time (Pielke et al. 1998). However, because the concurrent relationships between the two fields are dominated by the climate forcing, it is difficult to detect the weak feedbacks directly from observations of V'_t and T'_t. Therefore, it is more realistic to model V'_t using lagged vegetation and climate variables, and then to seek a relationship between the predicted "V'_t" and the observed T'_t [Equation (6)].

Table 2 shows the regression results for Equation (6). Overall, the r^2 statistics of the regression indicate that the equation explains about 5% of the total variance of temperature anomalies during the growing season (Table 2). Given the noisy nature of atmosphere signals, these low r^2 values are not a surprise. It is more important to note that the estimated relationships are statistically significant ($p < 0.05$) in most months for North America and in all the months for Eurasia (Table 2). Furthermore, values of these regression coefficients also indicate a pattern in which B_1 and B_3 tend to be positive while B_2 tends to be negative, which is particularly apparent over Eurasia (Table 2). This pattern is similar to that found in the coefficients for the climate forcing equation (Table 1) and therefore supports the findings that the vegetation signals have an influence on concurrent temperature anomalies (see below).

Yet the results of Table 2 do not exclude the possibility that the explanatory power about temperature variability contributed by vegetation anomalies can also be provided by other climate variables besides the one-month lagged temperature values. To examine this possibility, we extend Equation (6) as follows:

$$T'_t = B_1 V'_{t-1} + B_2 V'_{t-2} + \sum_{i=1}^{2} a_i T'_{t-i} + \sum_{i=1}^{2} c_i P'_{t-i} + \varepsilon_{2t}, \tag{7}$$

Table 2. Same as in Table 1, but for the regression results of the feedback equation (Equation (6)). Values in bold (italic) indicate that the results are significant at the 95% (90%) level, respectively.

	B_1	B_2	B_3	r^2
		(a) North America		
Jun	0.24	*2.55*	0.00	0.01
Jul	**3.20**	0.71	**0.20**	**0.06**
Aug	**4.71**	**–3.64**	**0.40**	**0.16**
Sep	**–9.57**	**13.1**	**0.09**	**0.03**
Oct	1.46	**–4.52**	**0.11**	**0.03**
		(b) Eurasia		
	B_1	B_2	B_3	r^2
Jun	**12.1**	**–7.55**	**–0.11**	**0.04**
Jul	**7.62**	**–4.03**	**0.13**	**0.07**
Aug	**8.19**	**–3.42**	**0.16**	**0.08**
Sep	**3.50**	**–3.97**	**0.19**	**0.03**
Oct	**5.45**	2.80	0.02	**0.02**

where *a*s and *c*s are constant coefficients. In Equation (7), if the lagged vegetation anomalies (V'_{t-1} and V'_{t-2}) provide information about current temperature variability (T'_t) that is not provided by lagged temperature and precipitation anomalies, B_1 and B_2 will be distinct from zero. In this case it suggests that vegetation anomalies Granger cause temperature variability[1] (W1).

We use two different techniques to test the Granger causality from vegetation to temperature as specified by Equation (7). Details of the two techniques are given in appendix A; they can also be found in previous studies (Granger and Huang 1997; Kaufmann and Stern 1997; Kaufmann et al. 2003; Wang et al. 2004; W1). Both methods give consistent results indicating that lagged NDVI anomalies have a significant ($p < 0.05$) statistical relationship to temperature variations during the growing season (Table 3). The coefficients B_1 and B_2 have the same pattern as described before, such that B_1 is mostly positive and B_2 is mostly negative (Table 3). These results suggest that the explanatory power of temperature variability contributed by vegetation is *not* qualitatively diminished by the inclusion of additional lagged climate variables in Equation (7). In other words, temperature anomalies do contain a component, although weak, that is uniquely related to vegetation variability.

The above panel-data approach only analyzes vegetation–temperature interactions in the average sense. However, it is also of interest to know how such vegetation feedbacks are spatially distributed. To address this question, we further estimate Equation (7) for each grid point in the domain and then test the corresponding Granger causality. Overall, the results show that in most regions the one-month lagged NDVI anomalies contribute positively (0.2°C, on average) to current temperature variability (Figure 4a), while the contributions from the two-month lagged NDVI anomalies are negative (–0.1°C, on average; Figure 4b).

[1] Although Equation (7) here explicitly uses a 2-month time lag, additional analyses using time lags of 3 or 4 months indicate qualitatively the same results as discussed in this section.

Table 3. Results of Granger causality tests for the generalized feedback equation (Equation (7)). B_1 and B_2 are regression coefficients associated with the two lagged NDVI anomalies; the ω statistics are results tested using the OLS algorithm; the S_{2a} and S_{3a} statistics show results tested using the out-of-sample forecast algorithm (their signs do *not* indicate the sign of the causal relationships under test). Values in bold (italic) indicate that the results are significant at the 95% (90%) level, respectively. See appendix A for detailed descriptions about these statistics.

	B_1	B_2	ω	S_{2a}	S_{3a}
			(a) North America		
Jun	0.39	−1.51	0.63	**−2.45**	*−1.59*
Jul	*2.92*	−0.05	*2.45*	**−1.70**	**−2.03**
Aug	**4.05**	**−3.45**	**3.57**	0.87	−0.62
Sep	**−5.74**	**6.56**	**3.80**	**−1.77**	**−2.34**
Oct	0.06	**−3.74**	*2.50*	**−1.62**	−0.60
			(b) Eurasia		
	B_1	B_2	ω	S_{2a}	S_{3a}
Jun	**7.02**	**−7.24**	**13.8**	**−2.05**	**−2.88**
Jul	**5.32**	**−5.47**	**12.8**	**−1.78**	**−2.22**
Aug	**6.48**	**−4.19**	**18.1**	**−4.11**	**−4.25**
Sep	**3.58**	−0.70	**4.17**	**−2.22**	*−1.49*
Oct	**4.04**	2.63	**9.05**	1.19	0.14

As a general rule, this pattern is stronger over the forests in the north and weakens in the southern portion near the grasslands (Figure 4). In particular, the most significant pattern is found in interior Asia (lower/central Siberia), over a broad region covering Lake Baikal (about 53°N, 104°E), Lake Balkhash (about 46°N, 76°E), and the northern Ural Mountains (about 60°N, 60°E) (Figures 4a,b). Part of this pattern also extends into northern Scandinavia (e.g., Finland) (Figures 4a,b). Over North America, however, vegetation effects are mainly found in a narrow range along the west coast of Canada (e.g., the Coast Mountains and the Canadian Rockies), although there is also a weak extension eastward to the Great Lakes (Figures 4a,b). The corresponding statistical significance levels for these patterns, tested by the Granger causality algorithm, are shown in Figure 4c.

The results of Figure 4 indicate a distinguishable spatial distribution of regions in which vegetation is closely coupled with temperature variability. In particular, it suggests that boreal forests over central Siberia may be a "hotspot" for vegetation–temperature coupling (analogous to the hotspots of soil moisture–precipitation coupling identified by Koster et al. 2004); on the other hand, vegetation feedbacks (over the forests) are much weaker in North America than Eurasia. Reasons for this apparent asymmetric pattern remain unknown. However, it is unlikely that this pattern is simply generated by random chance, because such signals would not necessarily be spatially coherent, nor would they have consistent positive/negative signs associated with them (Figure 4). In addition, it is noted that previous studies have reported many differences in climate–forest interactions between Eurasia and North America (e.g., Baldocchi et al. 2000; Eugster et al. 2000; Chapin et al. 2000). In particular, Zhou et al. (Zhou et al. 2001) indicate an asymmetry in the increased vegetation greenness, and its relation to climate variations, over North America (weaker) compared with Eurasia (stronger). While the

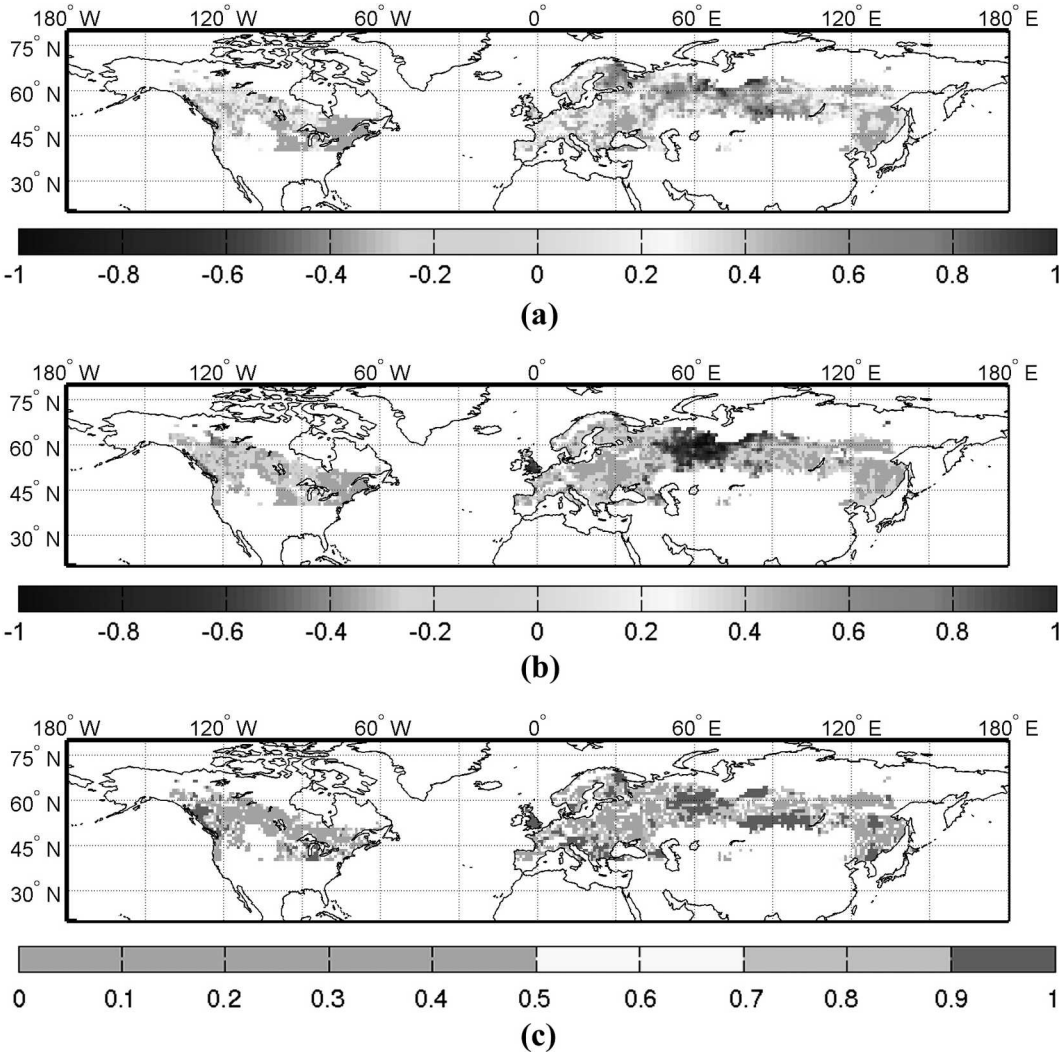

Figure 4. Temperature variations (°C) contributed from (top) one-month lagged NDVI anomalies and (middle) two-month lagged NDVI anomalies. (bottom) The statistical significance level tested by the Granger causality algorithm based on Equation (7).

asymmetric pattern of vegetation feedbacks detected in this study (Figure 4) may be related to the asymmetric pattern of vegetation greenness found in Zhou et al. (Zhou et al. 2001), a study of the relation between the intraseasonal variations (described here) and the long-term variations (described in Zhou et al. 2001) is beyond the scope of this study.

4. Theoretical analyses

The above statistical analyses indicate that vegetation–temperature interactions over the boreal forests can be described as a second-order dynamic system, which

features oscillatory variability at intraseasonal time scales. These characteristics are similar to those found between vegetation and precipitation over the midlatitude grasslands (W1). Therefore, it suggests that we may extend the stochastic modeling approach developed in W2 to investigate boreal forests. This section aims to address this question. In particular, we will begin by deriving a stochastic version of the climate forcing equation [Equation (3)]; then we will analyze its characteristics, discuss its physical implications, and finally extend the analyses to the feedback equation [Equation (6)].

4.1. Derivation of the climate forcing equation

As the major climate restraint over the boreal forests, changes in surface temperature will induce corresponding changes in vegetation. This relationship is generally defined by a long-term balance between the two fields, such that the changes of vegetation are proportional to the changes of temperature at long time scales (e.g., Myneni et al. 1997; Zhou et al. 2001). However, because the climate–vegetation system is a dynamic system, the above balance would not necessarily be reached "instantaneously." Depending on the time constant of the system, for instance, it may take some time for vegetation to fully adjust to the variations of the climate (Woodward 1987; Pielke et al. 1998).

A metric (denoted as E'), which determines whether the climate–vegetation system is in balance, may be defined as follows:

$$E'_t = \sum_{k=-\infty}^{t} \sigma^{t-k}\left(T'_k - \frac{1}{\gamma} V'_k\right), \tag{8}$$

where V' and T' represent anomalies of vegetation and temperature, respectively; the parameter γ ($0 < \gamma$, NDVI/temperature) represents the potential *long-term* relationship between the two fields (see below); and σ ($0 < \sigma < 1$) is a constant parameter, which can be understood as the decaying factor (or persistence rate) of E'.

The statistical implication of E' is qualitatively described here. As written, Equation (8) defines E' as a weighted summation (integral) of the *imbalances* between temperature and vegetation anomalies. If this quantity is positive (negative), it suggests that on average the preceding vegetation anomalies were lower (higher) than expected given their long-term relationship to temperatures; in order to eventually reach a climatological balance, therefore, vegetation is expected to increase (decrease) in the following months. As such, E' may provide information to predict future vegetation variability. To utilize this information, we introduce the following equation:

$$V'_t = \alpha V'_{t-1} + \beta E'_{t-1}, \tag{9}$$

where α ($0 < \alpha < 1$) is the persistence rate of vegetation anomalies, and β ($0 < \beta$, NDVI/temperature) represents the *short-term* responses of vegetation to temperature variations.

Together, Equations (8) and (9) represent a primitive model for vegetation dynamics, whose physical foundations will be discussed later in the paper. From the statistical point of view, though, this kind of model is generally known as an

"error correction" model in the literature (Stock and Watson 2003; Davidson and MacKinnon 2004). This is because, as written, Equation (8) simply measures the *errors* related to the deviation of past vegetation anomalies from their long-term balance with the climate forcing, while Equation (9) uses this measure to *correct* the future variability of vegetation. Equations (8) and (9) can be combined into one equation that explicitly involves only V' and T', that is,

$$V'_t = (\sigma + \alpha - \beta/\gamma)V'_{t-1} - \sigma\alpha V'_{t-2} + \beta T'_{t-1}. \tag{10}$$

Therefore, Equation (10) indicates that large-scale vegetation dynamics over the boreal forests can be modeled as a second-order system.

A weakness of Equation (10) is that it uses only lagged information to predict future vegetation variability. This approach can introduce errors because at monthly time scales a large portion of vegetation variance is induced by concurrent temperature anomalies (see the analyses of section 3). Because of this concern, we revise Equation (10) as follows to capture the "instantaneous" climate forcing:

$$V'_t = (\sigma + \alpha - \beta/\gamma)V'_{t-1} - \sigma\alpha V'_{t-2} + \beta T'_t. \tag{11}$$

The revision of Equation (11) generally has little effect on the intrinsic characteristics of the system because the latter is determined by the homogeneous structure of the model (i.e., the two lagged NDVI variables and their coefficients—Birkhoff and Rota 1989; Enders 1995). Yet we recognize that the revision requires some modifications to the error correction methodology, which we discuss in detail in appendix B. For simplicity, below we adopt Equation (11) as the ideal model in order to analyze the characteristics of the observed temperature–vegetation covariability.

4.2. Intraseasonal oscillatory variability

Compared with Equation (3), which represents the climate forcing equation in section 3, Equation (11) provides more details about the parameter structure of the climate–vegetation system. These details allow us to quantitatively explore the characteristic vegetation variability revealed by the statistical analyses in section 3. For instance, a quick check of the coefficients ($\sigma + \alpha - \beta/\gamma$, $-\sigma\alpha$, and β) of Equation (11) explains why the coefficients (A_1, A_2, and A_3) in Equation (3) have a regular positive–negative–positive pattern. Furthermore, since this pattern is important for determining whether or not the system is oscillatory [Equation (5)], these parameters (σ, α, β, and γ) also help to explain such oscillatory variability in a physically meaningful way.

First, the coefficients of Equation (11) indicate that Equation (5) can be rewritten as follows:

$$\Delta = (\sigma + \alpha - \beta/\gamma)^2 - 4\sigma\alpha. \tag{5'}$$

As discussed before, a negative value of Δ indicates that the system is oscillatory. Examining Equation (5′), it is clear that the value of Δ is determined by the factors of α, σ, and β/γ. Here β/γ ($0 < \beta/\gamma < 1$, unitless) represents a simple measure of how fast vegetation is produced or reduced (β) as it reaches its climatological balance with temperatures (γ). The value of β/γ is less than 1 because, as indicated

by the frequency analysis of section 3, vegetation's response to temperature has a higher magnitude at long time scales than at short time scales (Figure 3, top).

It can be analytically shown that for the same conditions, a larger value of α or β/γ increases the possibility that the system is oscillatory (see W2). To illustrate this point, we consider a system ("Normal") with the four parameters (σ, α, β, and γ) set to 0.4, 0.8, 0.005, and 0.011, respectively [these parameters will give 0.74, –0.32, and 0.005 for the three coefficients from Equation (3), which represent the typical values estimated from the observations; see Figure 2]. We can then decrease α by half ("Half-Alpha") or decrease β by half ("Half-Beta") to see how these changes influence the dynamic response of vegetation to an instantaneous temperature anomaly (i.e., we examine the impulse response function of the system).

Figure 5 shows the impulse response functions for the above scenarios. For the Normal system, the temperature anomaly at the initial time ($t = 0$) generates an instantaneous vegetation anomaly of magnitude 1 (normalized by β; same hereafter); this anomaly decreases and becomes negative within three months ($t = 3$), reaches its lowest point (about –0.12) at the fourth month ($t = 4$), and then starts to recover to zero (Figure 5, dark solid line). As such, it shows a clear oscillatory decaying trajectory. The Half-Alpha system has the same instantaneous response as the Normal configuration; however, the anomaly decays much faster. This fast-decaying characteristic shortens the period of the oscillation (about 5 months) and also reduces its magnitude (about –0.06 for the lowest value; Figure 5, gray

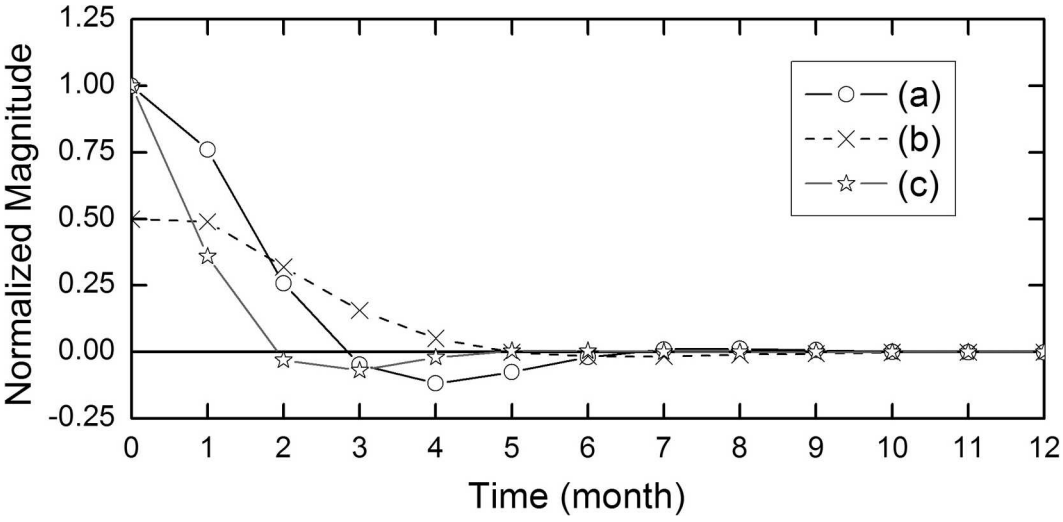

Figure 5. Impulse response functions of the climate forcing model (Equation 11) with different configurations: (a) the Normal configuration, in which the four parameters (σ, α, β, and γ) are set to 0.4, 0.8, 0.005, and 0.011, respectively; (b) the Half-Beta configuration, which has the same parameters as the Normal case but with the β parameter being set to 0.0025; (c) the Half-Alpha configuration, which has the same parameters as the Normal case but with the α parameter being set to 0.4. The Normal configuration gives the same overall coefficients as used in Figure 2 and Figure 3.

solid line). Finally, the Half-Beta system has a lower (0.5) instantaneous response to the temperature disturbance, which gradually decreases to zero with almost no sign of oscillatory behavior (Figure 5, gray dashed line).

The example given in Figure 5 verifies that increases of α or β increase the oscillatory variability of the climate–vegetation system. But why, physically, would the system be oscillatory in the first place? To address this question, note that increases of α or β also increase the long-term gain of vegetation anomalies related to increases of temperature. In fact, by substituting the vegetation and temperature terms in Equation (11) with two constants, V'_{const} and T'_{const}, respectively, the long-term balance between the two fields can be estimated as

$$V'_{\text{const}} = \gamma^* T'_{\text{const}}, \tag{12}$$

where

$$\gamma^* = \frac{\gamma}{[1 + (1 - \sigma)(1 - \alpha)\gamma/\beta]}. \tag{13}$$

In Equation (12), γ^* describes the *actual* long-term relationship between vegetation and temperature anomalies, which could possibly be as high as γ [Equation (13)] (for this reason, γ is called the *potential* long-term relationship). From Equation (13), it is easy to verify that γ^* is an increasing function of α and β, so that higher values of α and/or β induce higher values of γ^*. Equation (13) also indicates that a larger σ increases γ^*.

Physically, these results can be interpreted as follows: because suitable climate conditions are a "scarce" resource inasmuch as they do not occur at all times, if vegetation wants to enhance its gain during suitable growing periods (i.e., when temperatures increase), vegetation must increase its production rate (β) and/or become more persistent (α), which leads to not only larger overall growth but also to oscillatory behavior. To illustrate, we revise the above example (Normal, Half-Alpha, and Half-Beta) to examine how different parameters influence the long-term responses of vegetation to constant increases in temperature (i.e., the step response function; Figure 6). As shown, because it has a higher α and a higher β, the Normal configuration produces the highest "end state" vegetation amounts in all cases (Figure 6, dark solid line). More interestingly, it is noted that while the Half-Beta system generates lower vegetation anomalies than the Half-Alpha system at the beginning, its end state has higher vegetation amounts (Figure 6). The changes in the relative advantages between the Half-Beta system and the Half-Alpha system suggest an association with the "*K* selection" (generally slow-growing but long-lived species) and the "*r* selection" (generally fast-growing but short-lived species) strategies found in vegetation dynamics at long time scales (e.g., vegetation succession) (MacArthur and Wilson 1967; Gadgil and Solbrig 1972; Bonan 2002). Here, our results suggest that the physiological behavior that promotes growth during the presence of ideal, but short-lived, climate conditions may also induce enhanced intraseasonal oscillatory behavior; this appears to occur not only in boreal forest regions but also over grasslands as well (W1).

4.3. A physical explanation for E'

To derive the climate forcing equation [Equation (11)] as a second-order system, Equation (8) introduces the quantity E' based on its statistical relevance (i.e., error

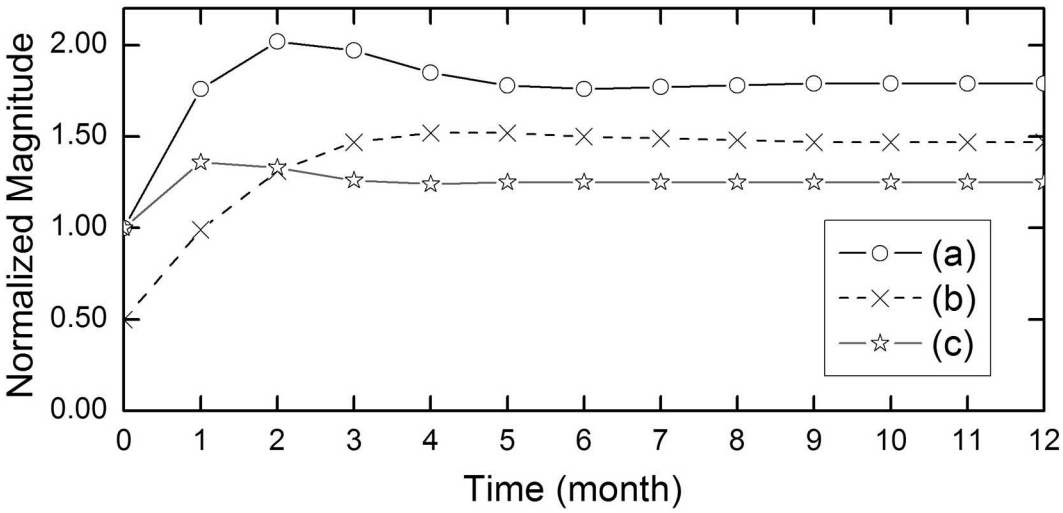

Figure 6. Same as in Figure 5, but shows the step response functions for (a) the Normal configuration, (b) the Half-Beta configuration, and (c) the Half-Alpha configuration.

correction; see above). On the other hand, since a statistical structure cannot physically influence vegetation–climate interactions in the real world, the agreement between the model and the observations suggest that there must be some physical phenomenon associated with E'. Here, we hypothesize that E' represents a measure of the *thermal energy* stored in the soil (and probably, the lower boundary layer of the atmosphere). We arrive at this hypothesis from the following thought experiment.

First, by assuming that soil has homogeneous thermal properties, thermal energy anomalies contained in soil, Q', can be expressed as

$$Q' = \rho_s C_s \delta \times T'_g, \tag{14}$$

where ρ_s is the soil density, C_s is the specific heat capacity, and δ is the thickness of the slab. Here, T'_g denotes the mean temperature anomaly of the soil, which is defined as (Hu and Islam 1995)

$$T'_g = \frac{1}{\delta} \int_0^{\delta} T'_s(z, t)\, dz, \tag{15}$$

where $T'_s(z, t)$ is the soil temperature anomaly at depth z and time t. Because the variations of deep ground temperature are generally small (Castelli et al. 1999), when δ is large enough, the changes of E' are mainly determined by the heat flux coming into the soil (G'; Hu and Islam 1995), that is,

$$\frac{dQ'}{dt} = \rho_s C_s \delta \frac{dT'_g}{dt} = G'(t). \tag{16}$$

Therefore, Equation (16) describes the thermal energy balance of the soil.

On the other hand, the soil heat flux anomaly G' can be derived from the surface energy budget (e.g., Cellier et al. 1996):

$$G' = R'_n - \mathrm{SH}' - \mathrm{LH}', \tag{17}$$

where R'_n is the net radiation energy anomaly, and SH′ and LH′ represent the sensible heat flux and the latent heat flux anomalies to the atmosphere, respectively. For simplicity, the energy stored in biochemical reactions is neglected.

The anomalous energy flux terms in Equation (17) can be linearly approximated using anomalies of vegetation, soil surface skin temperature, and surface air temperature. To simplify the derivation, here we approximate Equation (17) by qualitatively discussing how changes in V', T'_a, and T'_g will induce corresponding changes in G'. We directly use T'_g to proxy soil surface skin temperature $T'_s(0, t)$, because they are clearly related (Lin 1980; Hu and Islam 1995).

- *Vegetation* (V'): Vegetation can influence the soil heat flux G' by affecting the net radiation energy (R'_n) through the surface albedo feedback and by affecting the latent heat flux (LH′) via evapotranspiration (Pielke et al. 1998). Between these two mechanisms, the albedo feedback is generally less significant than evapotranspiration during the warm season when the soil is wet and dark (Hartmann 1994; Bounoua et al. 2000). Therefore, in warm seasons the overall effect of vegetation will generally tend to reduce G' (negative relationship).
- *Air Temperature* (T'_a): Warmer air can increase R'_n by emitting higher longwave radiation to warm the surface (Hartmann 1994); at the same time, higher air temperatures also reduce the surface–atmosphere temperature gradient and therefore reduce the sensible heat flux SH′ (Priestley 1959; Carson 1982). Both these relationships indicate that T'_a is positively related with G' in both ways.
- *Soil Temperature* (T'_g): Higher soil temperature implies that more energy is stored in soil. However, this energy anomaly is variable and can be dissipated by increasing outgoing longwave radiation (i.e., decreasing R'_n) and by increasing sensible heat SH′. Therefore, T'_g is negatively related with G'.

Based on the above discussions, therefore, Equation (17) can be approximated as follows:

$$G' = -aT'_g + (bT'_a - cV'), \tag{18}$$

where a, b, and c are constant (positive-definite) coefficients. For simplicity, the specific physical meanings of these "bulk" coefficients are neglected here; however, detailed discussions about these coefficients can be generally found in the corresponding literature (e.g., Hu and Islam 1995; Cellier et al. 1996; Castelli et al. 1999).

From Equations (18) and (16), it can be derived that

$$\frac{dQ'}{dt} = -\hat{a}Q' + (bT'_a - cV'), \tag{19}$$

where $\hat{a}$ is simply the original coefficient a divided by the factor $\rho_s C_s \delta$ [Equation (14)]. Rewriting Equation (19) in its convolution form gives

$$Q' = \int_0^t e^{-(t-\tau)/\hat{a}} [bT'_a(\tau) - cV'(\tau)]\, d\tau. \tag{20}$$

It is easy to see that Equation (20) represents a differential form of Equation (8), which defines E'. This suggests that E' represents a measure of anomalies in the soil thermal energy.

There are a few points about E' that need to be further clarified. First, when understood as soil thermal energy, the direct effect of E' upon vegetation growth is well known. For instance, soil warming experiments in midlatitude forests over North America (Melillo et al. 2002) and Europe (Jarvis and Linder 2000) report increases of vegetation, probably induced by the enhanced net nitrogen mineralization (Melillo et al. 2002) and other biochemical processes (e.g., nutrient cycles; Bonan 2002). In addition, in ecology, soil heat accumulation is most commonly expressed in growing degree days (GDDs; Baskerville and Emin 1969; Flannigan and Woodward 1994; McMaster and Wilhelm 1997; Wilhelm 1998), which are generally defined as accumulated daily temperature anomalies relative to a certain threshold (Baskerville and Emin 1969). When monthly anomalies (i.e., relative to the seasonal cycle) are considered, the link between GDDs and the quantity E' [Equation (8)] is apparent.

Second, it should be noted that the thermal balance of soil is also closely coupled with the thermal balance of the surface layer of the atmosphere. Indeed, the sensible heat flux SH$'$ to the atmosphere in Equation (17) plays a similar role as the heat flux G' to the soil (Cellier et al. 1996), and they can be looked at as net heat fluxes between air and soil partitioned according to the different thermal properties of the two media (Lettau 1951; Priestley 1959; Novak 1986). As such, E' can also be considered a (weighted) measure of the thermal energy in the lower boundary layer of the atmosphere.

The extension of E' to represent both soil and lower boundary layer atmospheric thermal energy allows us to make an analogy between the observed vegetation–climate interactions over boreal forests (which are related to surface energy balance; this study) and midlatitude grasslands (which are related to soil water balance; W1 and W2). From Equation (19), if there is an increase in surface temperature, the integrated heat content of the soil–atmosphere system will increase (this is equivalent to an increase in the soil moisture during periods of enhanced precipitation over the grasslands). In turn, vegetation activity will increase [Equation (9)], resulting in enhanced evaporation and a removal of excess heat. Alternatively, if there is an increase in vegetation activity, the net heat content of the system will decrease (via an increase in evapotranspiration). This will result in a decrease in the sensible heat term to offset the increase in the evaporative term. At the same time, a decrease in the sensible heat term requires a decrease in the canopy temperatures, which will result in a decrease in vegetation growth [Equation (9)].

It is important to note that the above analogy (and the model itself) is only intended to give a qualitative explanation for the *observed* covariability between temperature and vegetation. For this purpose, the model highly simplifies the

climatological/ecological processes that may be involved. For instance, it may be better to treat the atmosphere and soil as two interacting thermal reservoirs, and to distinguish the response of vegetation to atmospheric thermal energy (e.g., concurrent temperature anomalies) and to soil heat (e.g., lagged temperatures). However, the simple form of the statistical model [e.g., Equation (3)] may not allow these details to be fully retrieved. Therefore, by analogy we simply emphasize that temperatures can have persistent effects on vegetation, while vegetation itself may provide a negative feedback to reduce such thermal energy. It is recognized that further process-based studies are necessary to assess the validity of the mechanisms proposed here.

4.4. Feedbacks to the atmosphere

Thermal energy stored in soil may persist and warm/cool the surface in the following months (Chen and Kumar 2004; Hu and Feng 2004). This suggests that the total variability of surface temperature can have contributions both from the external climate forcing and from the local surface feedbacks. As such, it can be described as follows:

$$T'_t = \theta E'_{t-1} + \varepsilon_{2t}, \tag{21}$$

where θ ($0 < \theta < 1$) is a constant coefficient that indicates the strength of the feedback, and ε_{2t} is the external temperature variability, which is assumed to be a random process (i.e., white noise). By substituting E'_{t-1} in Equation (21) using vegetation and temperature anomalies, it can be shown (see appendix B) that

$$T'_t = \frac{\theta(1-\beta/\gamma)}{\beta} V'_{t-1} - \frac{\theta\alpha}{\beta} V'_{t-2} + \theta T'_{t-1} + \varepsilon_{2t}. \tag{22}$$

Equation (22) provides the "theoretical" version of Equation (6), which is the feedback function in section 3. Overall, it indicates that the one-month lagged vegetation anomalies (V'_{t-1}) have a positive relationship with current temperature variations, while the two-month lagged vegetation anomalies (V'_{t-2}) have a negative relationship with the latter. This pattern is consistent with the findings of the statistical analyses (Table 2, Table 3, and Figure 4). The derivation of Equation (22) also suggests the reason for this pattern. Qualitatively, this pattern arises because Equation (22) attempts to infer the quantity E'_{t-1} from the variability of V'_{t-1}; on the other hand, the variability of V'_{t-1} also has a contribution from V'_{t-2}, which is independent of E'_{t-1} [Equation (9); appendix B). Therefore, it is necessary to subtract the persistent component of V'_{t-2} from V'_{t-1} to provide a better estimate of E'_{t-1}, as indicated by the corresponding positive/negative coefficients in Equation (22).

The above model derivation also indicates that the influence of vegetation suggested by Equation (6) [or Equation (22)] should be carefully interpreted. For instance, the positive relationship between V'_{t-1} and T'_t may not indicate that "vegetation raises temperature" (i.e., the albedo feedback); nor does the negative relationship between V'_{t-2} and T'_t indicate that "vegetation reduces temperature" (i.e., the evapotranspiration feedback). Instead, these relationships *together* represent the thermal inertial effects (E'_{t-1}) on current temperature variations. At the same time, because the effects of vegetation are mainly to remove thermal energy

from the surface during the warm season (see above), these influences, taken *together*, will tend to reduce surface temperatures. This example highlights the challenges of detecting vegetation feedbacks from observations; however, it also suggests that by carefully analyzing the "fingerprints" of vegetation on climate variability, we may be able to overcome these difficulties.

5. Conclusions

This study extends the methodologies of W1 and W2 to investigate climate–vegetation interactions over the boreal forests. Statistical analyses indicate that the relationship between observed temperature and NDVI anomalies can be described as a second-order dynamic system. From the perspective of climate forcing on vegetation variability, this means that vegetation growth is not only influenced by concurrent temperature variations, but also by its own status during the preceding two months. A statistical model with these specifications explains more than 40% of the variance of NDVI anomalies for boreal forests over both North America and Eurasia. In particular, it is found that the one-month lagged NDVI anomalies contribute positively to current vegetation variations, while the contributions from the two-month lagged NDVI anomalies are negative. A second-order system with such coefficient patterns can have intrinsic oscillatory variability, which is verified for NDVI anomalies at most grid points in the domain of analysis. With the estimated regression coefficients, the mean oscillation period for boreal forests is about seven months.

When the effects of vegetation on temperature variability are considered, the two lagged NDVI anomalies also contribute statistically significant information to the current temperature variations, which otherwise cannot be found in lagged temperature and precipitation anomalies over the same period. This suggests that NDVI anomalies "Granger cause" variations in temperature. It is also found that the regression coefficients between the one-month lagged NDVI anomalies and current temperature variations are generally positive, and those between the two-month lagged NDVI anomalies and current temperature variations tend to be negative. These vegetation feedbacks are further verified by Granger causality analyses for each grid point in the domain with the most significant vegetation–temperature couplings found over the boreal forests in lower and central Siberia (interior Asia).

To explain the characteristics of the observed temperature–vegetation interactions, a stochastic model is derived based on the principle of surface thermal energy balance. The model assumes that the long-term relationship between temperature and vegetation anomalies is based upon a thermal balance within the soil and the lower boundary layer of the atmosphere. Deviations from this long-term relationship in either the temperature and/or vegetation fields will generate corresponding thermal energy anomalies, which in turn induce changes of vegetation (as well as temperatures) to reduce such short-term imbalances so that the system can adjust to its long-term balance. This assumption is consistent with many biogeophysical mechanisms known in the literature. For instance, it has been long recognized that thermal energy in soil can influence vegetation growth, while the negative effects of vegetation on such soil heat storage can be directly derived from the surface energy budget.

Based on the above assumption, the stochastic model can be derived as a pair of second-order difference equations that have the same form as their statistical counterparts. These equations suggest that the patterns of the estimated regression coefficients (e.g., the positive/negative values associated with the lagged NDVI anomalies) can be explained by a set of parameters that represent the dynamic characteristics of the climate–vegetation system. This makes the stochastic model useful to investigate possible physical mechanisms for the observed temperature–vegetation covariability. For instance, analyses of the climate forcing equation suggest that in order to enhance its long-term gain during suitable growing conditions, vegetation may opt to grow faster and/or become more persistent; at the same time, these characteristics can make vegetation temporarily "overshoot" its long-term balance with the climate forcing, which in turn induces intrinsic oscillatory variability. Analyses of the feedback function also indicate that the observed causal effects of vegetation on temperatures likely reflect the inertial effects of thermal energy of the surface reservoir; the role vegetation plays in this scenario is mainly to dissipate such thermal energy and therefore reduce surface temperatures.

It is important to note that we do not argue that the above hypothesized mechanism is the only way that vegetation interacts with climate over the boreal regions. The statistical/stochastic models represent a highly simplified scenario of the climate–vegetation interactions that may occur in the real world, and they capture only about half of the variance of the observed NDVI anomalies and less than 10% of that of the temperature anomalies. Furthermore, the results of this study are also restrained by the datasets used in the analyses. The monthly time scales of the data may prevent us from distinguishing "fast" (i.e., submonthly) vegetation feedbacks, directly via albedo or evapotranspiration regulations, on surface climate variability. At the same time, the feedback pathway via the thermal energy balance represents a relatively "slow" process, which may be easier to capture at intraseasonal time scales. Therefore, it is recognized that findings of this study need to be further investigated by dedicated and process-based approaches in the future.

Acknowledgments. This work was supported in part by the NASA Earth Science Enterprise. The views expressed herein are those of the authors and do not necessarily reflect the views of NASA. The authors are thankful to two anonymous reviewers for their constructive comments and suggestions. GISS temperature data were provided by the NASA GISS Surface Temperature Analysis from their Web site (http://data.giss.nasa.gov/gistemp/). CMAP precipitation data were provided by the CIRES Climate Diagnostics Center and NOAA/ESRL/PSD, Boulder, Colorado, from their Web site at (http://www.cdc.noaa.gov/). We also would like to thank Dr. C. J. Tucker for providing the GIMMS NDVI data.

Appendix A

Algorithms to Test Granger Causality

This appendix introduces two algorithms to test the existence of Granger causality in statistical models like Equation (7). To facilitate discussion, Equation (7) is rewritten here as Equation (A1).

$$T'_t = B_1 V'_{t-1} + B_2 V'_{t-2} + \sum_{i=1}^{2} a_i T'_{t-i} + \sum_{i=1}^{2} c_i P'_{t-i} + \varepsilon_{2t}. \quad \text{(A1)}$$

Because Equation (A1) uses the full information set (lagged anomalies of vegetation, temperature, and precipitation) to predict temperature variations, it is often referred to as the *unrestricted* model. On the other hand, the corresponding *restricted* model is given by Equation (A2):

$$T'_t = \sum_{i=1}^{2} a'_i T'_{t-i} + \sum_{i=1}^{2} c'_i P'_{t-i} + \varepsilon'_{2t}. \quad \text{(A2)}$$

Therefore, the purpose of the Granger causality test is to determine whether by eliminating vegetation information from the unrestricted model it will deteriorate its explanation power/prediction skill in a statistically significant fashion.

A.1. Ordinary least squares (OLS)

As discussed above, the null hypothesis here is that eliminating the lagged values of NDVI from Equation (A1) does not reduce its explanatory power in a statistically meaningful fashion. To test this hypothesis, a statistic is constructed as follows:

$$\omega = \frac{(\mathrm{RSS}_r - \mathrm{RSS}_u)/s}{\mathrm{RSS}_u/(L-k)}, \quad \text{(A3)}$$

where RSS represents the residual sum of squares, while the subscripts r and u refer to the "restricted" and the "unrestricted" model [i.e., Equations (A2) and (A1)], respectively; s is the number of coefficients restricted to zero in Equation (A2); L is the number of total observations (e.g., $L = 176 \times 19$ for North America); and k is the number of regressors in Equation (A1). The test statistic (ω) can be evaluated against an F distribution with s and $L - k$ degrees of freedom in the numerator and denominator, respectively. High values of ω that exceed the 5% threshold indicate that NDVI anomalies Granger cause precipitation variability.

A.2. Out-of-sample forecast

First, we use the following procedure to make out-of-sample forecasts for the observed precipitation variations.

(i) Eliminate one box (e.g., j) from the panel, which subsequently decreases the size of the panel by 1 (e.g., 70–1).
(ii) Use data from the remaining boxes ($i = 1 \sim 70$, $i \neq j$) to estimate the regression coefficients for Equation (A1) and Equation (A2), respectively.
(iii) Use the regression coefficients estimated in (ii) to make a forecast for the j box. The forecasts generated with Equations (A1) and (A2) are denoted as $\hat{P}^j_{m,U}$ and $\hat{P}^j_{m,R}$, respectively.
(iv) Repeat the above processes for each of the boxes in the panel.

Next, we compare the accuracy of the two sets of out-of-sample forecasts, by the unrestricted model Equation (A1) and by the restricted model Equation (A2), using the following metric:

$$I_+(d_t) = \begin{cases} 1, & d_t > 0 \\ 0, & \text{otherwise,} \end{cases} \tag{A4}$$

where

$$d_t = [\text{Precip}_m^i - \hat{P}_{m,U}^i]^2 - [\text{Precip}_m^i - \hat{P}_{m,R}^i]^2. \tag{A5}$$

To test the null hypothesis that the accuracy of the out-of-sample forecasts is equal, two statistics (Diebold and Mariano 1995) are constructed as follows:

$$S_{2a} = \frac{\sum_{t=1}^{L} I_+(d_t) - 0.5L}{\sqrt{0.25L}}, \tag{A6}$$

$$S_{3a} = \frac{\sum_{t=1}^{L} I_+(d_t)\text{rank}(|d_t|) - L(L+1)/4}{\sqrt{L(L+1)(2L+1)/24}}, \tag{A7}$$

where L is the number of total observations (e.g., $L = 70 \times 19$). The S_{2a} and S_{3a} statistics can be evaluated against a Student's t distribution with degrees of freedom equal to $(L - 1)$. Note that if the forecast errors generated by the unrestricted model [Equation (A1)] are smaller than those of the restricted model [Equation (A2)], the test statistics will be *negative*. Therefore, only negative values of S_{2a} and S_{3a} that are lower than the 5% threshold (which itself is negative) indicate the presence of Granger causality.

Appendix B

Derivation of Equation (11) and Equation (22)

B.1. Equation (11)

To incorporate the concurrent temperature anomalies into the model, we revise Equation (8) as follows:

$$V'_t = \alpha V'_{t-1} + \beta T'_t + \sigma\beta E'_{t-1}. \tag{B1}$$

For the sake of convenience, we also rewrite Equation (9) here as Equation (B2):

$$E'_t = \sum_{k=-\infty}^{t} \sigma^{t-k}\left(T'_k - \frac{1}{\gamma} V'_k\right). \tag{B2}$$

From Equations (B1) and (B2), it can be derived that

$$V'_t = (\sigma + \alpha - \sigma\beta/\gamma)V'_{t-1} - \sigma\alpha V'_{t-2} + \beta T'_t. \tag{B3}$$

To write Equation (B3) in the exact form of Equation (11), it is noted that

$$\begin{aligned}\beta T'_t + \sigma\beta E'_{t-1} &= \beta(T'_t + \sigma E'_{t-1}) \\ &= \beta\left\{ T'_t + \sigma\left[\sum_{k=-\infty}^{t-1} \sigma^{t-1-k}\left(T'_k - \frac{1}{\gamma} V'_k \right) \right] \right\} \\ &= \beta\left(T'_t + \sum_{k=-\infty}^{t-1} \sigma^{t-k} T'_k - \frac{1}{\gamma} \sum_{k=-\infty}^{t-1} \sigma^{t-k} V'_k \right) \\ &= \beta\left(\sum_{k=-\infty}^{t} \sigma^{t-k} T'_k - \frac{1}{\gamma/\sigma} \sum_{k=-\infty}^{t-1} \sigma^{t-1-k} V'_k \right) \\ &= \beta\left(\sum_{k=-\infty}^{t} \sigma^{t-k} T'_k - \frac{1}{\gamma'} \sum_{k=-\infty}^{t-1} \sigma^{t-1-k} V'_k \right), \end{aligned} \tag{B4}$$

where

$$\gamma' = \gamma/\sigma. \tag{B5}$$

Equation (B4) indicates that the long-term relationship between accumulated temperature anomalies and accumulated vegetation anomalies now are defined by γ', which is generally higher than γ. This change may be because Equation (B1) considers only the "instantaneous" effects of temperature on vegetation but neglects the corresponding instantaneous feedbacks, which itself deviates from the idea of error correction. Nevertheless, this problem does not influence the overall characteristics of the model. Plugging Equation (B5) into Equation (B3) gives

$$V'_t = (\sigma + \alpha - \beta/\gamma')V'_{t-1} - \sigma\alpha V'_{t-2} + \beta T'_t, \tag{B6}$$

which has the same form as Equation (12).

B.2. Equation (22)

To represent E'_{t-1} using vegetation and temperature terms, note that Equation (B1) can be rearranged as

$$\sigma\beta E'_{t-1} = V'_t - \alpha V'_{t-1} - \beta T'_t. \tag{B7}$$

Plugging Equation (B3) into Equation (B7) to substitute for V'_t allows us to derive

$$E'_{t-1} = \frac{(1 - \beta/\gamma)}{\beta} V'_{t-1} - \frac{\alpha}{\beta} V'_{t-2}. \tag{B8}$$

Equation (B8) represents a "perfect" situation in which E'_{t-1} can be expressed by only lagged NDVI anomalies. However, analyses of the observed data often indicate a persistence effect of lagged temperature anomalies on their current variations (see Table 2). As such, Equation (22) correspondingly includes a lagged temperature term to better match the observations. Clearly, this revision will not affect our discussions about vegetation feedbacks.

References

Baldocchi, D., F. M. Kelliher, T. A. Black, and P. Jarvis, 2000: Climate and vegetation controls on boreal zone energy exchange. *Global Change Biol.,* **6** (Suppl.), 69–83.

Baskerville, G. L., and P. Emin, 1969: Rapid estimation of heat accumulation from maximum and minimum temperature. *Ecology,* **50,** 514–517.

Birkhoff, G., and G.-C. Rota, 1989: *Ordinary Differential Equations.* Wiley, 399 pp.

Bonan, G. B., 2002: *Ecological Climatology, Concepts and Applications.* Cambridge University Press, 678 pp.

Bounoua, L., G. J. Collatz, S. O. Los, P. J. Sellers, D. A. Dazlich, C. J. Tucker, and D. A. Randall, 2000: Sensitivity of climate to changes in NDVI. *J. Climate,* **13,** 2277–2292.

Braswell, B. H., D. S. Schimel, E. Linder, and B. Moore III, 1997: The response of global terrestrial ecosystems to interannual temperature variability. *Science,* **278,** 870–872.

Brunsell, N. A., 2006: Characterization of land-surface precipitation feedback regimes with remote sensing. *Remote Sens. Environ.,* **100,** 200–211.

Budyko, M. I., 1974: *Climate and Life.* Academic Press, 508 pp.

Buermann, W., B. Anderson, C. J. Tucker, R. E. Dickinson, W. Lucht, C. S. Potter, and R. B. Myneni, 2003: Interannual covariability in Northern Hemisphere air temperatures and greenness associated with El Niño-Southern Oscillation and the Arctic Oscillation. *J. Geophys. Res.,* **108,** 4396, doi:10.1029/2002JD002630.

Castelli, F., D. Entekhabi, and E. Caporali, 1999: Estimation of surface heat flux and an index of soil moisture using adjoint-state surface energy balance. *Water Resour. Res.,* **35,** 3115–3125.

Carson, D. J., 1982: Current parameterizations of land surface processes in atmospheric general circulation models. *Land Surface Processes in Atmospheric General Circulation Models,* P. S. Eagleson, Ed., Cambridge University Press, 67–108.

Cellier, P., G. Richard, and P. Robin, 1996: Partition of sensible heat fluxes into bare soil and the atmosphere. *Agric. For. Meteor.,* **82,** 245–265.

Chapin, F. S., III, and Coauthors, 2000: Arctic and boreal ecosystems of western North America as components of the climate system. *Global Change Biol.,* **6** (Suppl.), 211–223.

Chen, J., and P. Kumar, 2004: A modeling study of the ENSO influence on the terrestrial energy profile in North America. *J. Climate,* **17,** 1657–1670.

Davidson, R., and J. G. MacKinnon, 2004: *Econometric Theory and Methods.* Oxford University Press, 768 pp.

Diebold, F. X., and R. S. Mariano, 1995: Comparing predictive accuracy. *J. Bus. Econ. Stat.,* **13,** 253–263.

Enders, W., 1995: *Applied Econometric Time Series.* Wiley & Sons, 448 pp.

Eugster, W., and Coauthors, 2000: Land-atmosphere energy exchange in Arctic tundra and boreal forest: Available data and feedbacks to climate. *Global Change Biol.,* **6** (Suppl.), 84–115.

Flannigan, M. D., and F. I. Woodward, 1994: Red pine abundance—Current climate control and responses to future warming. *Can. J. For. Res.,* **24,** 1166–1175.

Frankignoul, C., A. Czaja, and B. L'Heveder, 1998: Air–sea feedback in the North Atlantic and surface boundary conditions for ocean models. *J. Climate,* **11,** 2310–2324.

Friedl, M. A., and Coauthors, 2002: Global land cover mapping from MODIS: Algorithms and early results. *Remote Sens. Environ.,* **83** (1–2), 287–302.

Gadgil, M., and O. T. Solbrig, 1972: The concept of r- and K-selection: Evidence from wild flowers and some theoretical considerations. *Amer. Nat.,* **106,** 14–31.

Granger, C. W. J., 1969: Investigating causal relations by econometric models and cross-spectral methods. *Econometrica,* **37,** 424–438.

——, 1980: Testing for causality, a personal viewpoint. *J. Econ. Dyn. Control,* **2,** 329–352.

——, and L. Huang, 1997: Evaluation of Panel Data Models: Some suggestions from time series. discussion paper, Department of Economics, University of California, San Diego, 29 pp.

Hansen, J., R. Ruedy, J. Glascoe, and M. Sato, 1999: GISS analysis of surface temperature change. *J. Geophys. Res.,* **104,** 30 997–31 022.

——, ——, M. Sato, M. Imhoff, W. Lawrence, D. Easterling, T. Peterson, and T. Karl, 2001: A closer look at United States and global surface temperature change. *J. Geophys. Res.,* **106,** 23 947–23 963.

Hartmann, D. L., 1994: *Global Physical Climatology.* Academic Press, 411 pp.

Hu, Q., and S. Feng, 2004: A role of the soil enthalpy in land memory. *J. Climate,* **17,** 3633–3643.

Hu, Z., and S. Islam, 1995: Prediction of ground surface temperature and soil moisture content by the force-restore method. *Water Resour. Res.,* **31,** 2531–2539.

Jarvis, P., and S. Linder, 2000: Constraints to growth of boreal forests. *Nature,* **405,** 904–905.

Jenkins, G. M., and D. G. Watts, 1968: *Spectral Analysis and Its Applications.* Holden-Day, 525 pp.

Kaufmann, R. K., and D. I. Stern, 1997: Evidence for human influence on climate from hemispheric temperature relations. *Nature,* **388,** 39–44.

——, L. Zhou, R. B. Myneni, C. J. Tucker, D. Slayback, N. V. Shabanov, and J. Pinzon, 2003: The effect of vegetation on surface temperature: A statistical analysis of NDVI and climate data. *Geophys. Res. Lett.,* **30,** 2147, doi:10.1029/2003GL018251.

Koster, R. D., and Coauthors, 2004: Regions of strong coupling between soil moisture and precipitation. *Science,* **305,** 1138–1140.

Lettau, H. H., 1951: Theory of surface temperature and heat transfer oscillations near a level ground surface. *Eos, Trans. Amer. Geophys. Union,* **32,** 189–200.

Lin, J. D., 1980: On the force-restore method for prediction of ground surface temperature. *J. Geophys. Res.,* **85,** 3251–3254.

Liu, Z., M. Notaro, J. Kutzbach, and N. Liu, 2006: An observational assessment of global vegetation–climate feedbacks. *J. Climate,* **19,** 787–814.

Lotsch, A., M. A. Friedl, B. T. Anderson, and C. J. Tucker, 2003: Coupled vegetation-precipitation variability observed from satellite and climate records. *Geophys. Res. Lett.,* **30,** 1774, doi:10.1029/2003GL017506.

Lucht, W., and Coauthors, 2002: Climatic control of the high-latitude vegetation greening trend and Pinatubo effect. *Science,* **296,** 1687–1689.

MacArthur, R. H., and E. O. Wilson, 1967: *The Theory of Island Biogeography.* Princeton University Press, 203 pp.

McMaster, G. S., and W. W. Wilhelm, 1997: Growing degree-days: One equation, two interpretations. *Agric. For. Meteor.,* **87,** 291–300.

——, and ——, 1998: Is soil temperature better than air temperature for predicting winter wheat phenology? *Agron. J.,* **90,** 602–607.

Melillo, J. M., and Coauthors, 2002: Soil warming and carbon-cycle feedbacks to the climate system. *Science,* **298,** 2173–2176.

Myneni, R. B., C. D. Keeling, C. J. Tucker, G. Asrar, and R. R. Nemani, 1997: Increased plant growth in the northern high latitudes from 1981 to 1991. *Nature,* **386,** 698–702.

Notaro, M., Z. Liu, and J. W. Williams, 2006: Observed vegetation–climate feedbacks in the United States. *J. Climate,* **19,** 763–786.

Novak, M. D., 1986: Theoretical values of daily atmospheric and soil thermal admittances. *Bound.-Layer Meteor.,* **24,** 17–34.

Pielke, R. A., R. Avissar, M. Raupach, A. J. Dolman, X. Zeng, and A. S. Denning, 1998: Interactions between the atmosphere and terrestrial ecosystems: Influence on weather and climate. *Global Change Biol.,* **4,** 461–475.

Priestley, C. H. B., 1959: *Turbulent Transfer in the Lower Atmosphere.* University of Chicago Press, 130 pp.

Sellers, P. J., and Coauthors, 1997: Modeling the exchanges of energy, water, and carbon between continents and the atmosphere. *Science,* **275,** 502–509.

Stock, J. H., and M. W. Watson, 2003: *Introduction to Econometrics.* Addison-Wesley, 696 pp.

Tucker, C. J., J. E. Pinzon, M. E. Brown, D. Slayback, E. W. Pak, R. Mahoney, E. Vermote, and N. El Saleous, 2005: An extended AVHRR 8-km NDVI data set compatible with MODIS and SPOT vegetation NDVI data. *Int. J. Remote Sens.,* **26,** 4485–4498.

Walter, H., 1985: *Vegetation of the Earth and Ecological Systems of the Geo-Biosphere.* Springer-Verlag, 318 pp.

Wang, W., B. T. Anderson, R. K. Kaufmann, and R. B. Myneni, 2004: The relation between the North Atlantic Oscillation and SSTs in the North Atlantic basin. *J. Climate,* **17,** 4752–4759.

——, ——, P. Nathan, R. K. Kaufmann, and R. B. Myneni, 2006a: Feedbacks of vegetation on summertime climate variability over the North American Grasslands. Part I: Statistical analysis. *Earth Interactions,* **10.** [Available online at http://EarthInteractions.org.]

——, ——, D. Entekhabi, D. Huang, R. K. Kaufmann, and R. B. Myneni, 2006b: Feedbacks of vegetation on summertime climate variability over the North American Grasslands. Part II: A coupled stochastic model. *Earth Interactions,* **10.** [Available online at http://EarthInteractions.org.]

Woodward, F. I., 1987: *Climate and Plant Distribution.* Cambridge University Press, 174 pp.

Xie and Arkin, 1997: Global precipitation: A 17-year monthly analysis based on gauge observations, satellite estimates, and numerical model outputs. *Bull. Amer. Meteor. Soc.,* **78,** 2539–2558.

Zhou, L., C. J. Tucker, R. K. Kaufmann, D. Slayback, N. V. Shabanov, and R. B. Myneni, 2001: Variations in northern vegetation activity inferred from satellite data of vegetation index during 1981 to 1999. *J. Geophys. Res.,* **106,** 20 069–20 083.

——, R. K. Kaufamann, Y. Tian, R. B. Myneni, and C. J. Tucker, 2003: Relation between interannual variations in satellite measures of northern forest greenness and climate between 1982 and 1999. *J. Geophys. Res.,* **108,** 4004, doi:10.1029/2002JD002510.